JOURNAL OF GEOPHYSICAL RESEARCH, VOL. 113, E00B24, doi:10.1029/2008JE003134, 2008

Click Here for Full Article

Felsic highland crust on Venus suggested by Galileo Near-Infrared Mapping Spectrometer data

George L. Hashimoto,[1] Maarten Roos-Serote,[2] Seiji Sugita,[3] Martha S. Gilmore,[4] Lucas W. Kamp,[5] Robert W. Carlson,[5] and Kevin H. Baines[5]

Received 2 March 2008; revised 29 July 2008; accepted 18 September 2008; published 31 December 2008.

[1] We evaluated the spatial variation of Venusian surface emissivity at 1.18 μm wavelength and that of near-surface atmospheric temperature using multispectral images obtained by the Near-Infrared Mapping Spectrometer (NIMS) on board the Galileo spacecraft. The Galileo NIMS observed the nightside thermal emission from the surface and the deep atmosphere of Venus, which is attenuated by scattering from the overlying clouds. To analyze the NIMS data, we used a radiative transfer model based on the adding method. Although there is still an uncertainty in the results owing to the not well known parameters of the atmosphere, our analysis revealed that the horizontal temperature variation in the near-surface atmosphere is no more than ±2 K on the Venusian nightside and also suggests that the majority of lowlands likely has higher emissivity compared to the majority of highlands. One interpretation for the latter result is that highland materials are generally composed of felsic rocks. Since formation of a large body of granitic magmas requires water, the presence of granitic terrains would imply that Venus may have had an ocean and a mechanism to recycle water into the mantle in the past.

Citation: Hashimoto, G. L., M. Roos-Serote, S. Sugita, M. S. Gilmore, L. W. Kamp, R. W. Carlson, and K. H. Baines (2008), Felsic highland crust on Venus suggested by Galileo Near-Infrared Mapping Spectrometer data, *J. Geophys. Res.*, *113*, E00B24, doi:10.1029/2008JE003134.

1. Introduction

[2] Venus is the nearest neighbor of Earth, and these twins are close in mass, size, and bulk composition. However, the surface environment of Venus is completely different from that of Earth, where the mean surface temperature is 735 K and water is almost absent. In contrast, the Earth surface is covered with ocean and is habitable. It is not clear whether the surface environments on these twin planets differed from beginning or they evolved from a similar environment into the current different states. Understanding the evolution of these twin planets is one of the most important and elusive problems in planetary climatology.

[3] The chemical and mineralogical composition of the Venus surface can provide valuable information on the climatic evolution of Venus. If geologic signatures that are produced only under unique conditions are found in the chemical and mineralogical composition, they could be used to reconstruct the Venus paleoenvironment. Additionally, a global map of surface composition will be a very important diagnostic of bulk planetary composition, chemical differentiation, and evolution of the planetary interior.

[4] It has been also argued that the controlling mechanism of the present Venus surface environment is a connection between the atmosphere and the chemical characteristics of planetary surface [e.g., *Hashimoto and Abe*, 2005, and references therein]. The high surface temperature of Venus enhances the importance of the gas-solid reactions on the planetary surface in controlling the atmospheric composition, including infrared-active species which control the greenhouse effect. Venus climate models that combine chemical reaction and radiative transfer in the atmosphere have demonstrated that such a coupling between surface chemical reactions and greenhouse effect will play an important role in controlling the surface environment [e.g., *Hashimoto and Abe*, 2000; *Bullock and Grinspoon*, 2001].

[5] However, chemical characteristics of the Venus surface are not well constrained. In situ measurements of the surface using gamma-ray and X-ray fluorescence spectroscopy were performed by Venera and Vega landers [*Surkov et al.*, 1984, 1986, 1987], but it is difficult to infer the global characteristics from lander data collected at 7 sites on the planet. Although the radar reflectivity and radiothermal emissivity were measured nearly globally [e.g., *Pettengill et al.*, 1982, 1992], origins of the microwave emissivity differences are highly controversial and appear to be related to both grain size and dielectric constant of constituent

[1] Laboratory for Earth and Planetary Atmospheric Science, Organization of Advanced Science and Technology, Kobe University, Kobe, Japan.
[2] Lisbon Astronomical Observatory, Lisbon, Portugal.
[3] Department of Complexity Science and Engineering, Graduate School of Frontier Science, University of Tokyo, Kashiwa, Japan.
[4] Department of Earth and Environmental Sciences, Wesleyan University, Middletown, Connecticut, USA.
[5] Jet Propulsion Laboratory, California Institute of Technology, Pasadena, California, USA.

Copyright 2008 by the American Geophysical Union.
0148-0227/08/2008JE003134$09.00

minerals [e.g., *Campbell et al.*, 1997; *Pettengill et al.*, 1997]. We need a new observation capable of determining the chemical and mineralogical composition of the Venus surface.

[6] It has been discovered that thermal emission from the surface of Venus is detectable at the CO_2-free windows in the near-infrared wavelengths (0.85, 0.90, 1.01, 1.10, and 1.18 μm) [e.g., *Carlson et al.*, 1993a, 1993b; *Meadows and Crisp*, 1996; *Baines et al.*, 2000]. Thermal emissivity is a function of surface temperature, grain size, and mineral composition. Previous investigations of surface emissivity using Earth-based telescopic data have demonstrated variations that appear to be correlated with topography and therefore surface temperature [*Lecacheux et al.*, 1993; *Meadows and Crisp*, 1996]. Although the variations in the surface emissivity have been investigated, no signature of surface emissivity differences was found at near-infrared wavelengths in contrast with the microwave wavelengths [*Lecacheux et al.*, 1993; *Meadows and Crisp*, 1996]. However, these analyses neglect multiple reflection between the planetary surface and the clouds which has been demonstrated to significantly obscure variations in surface emissivity [*Moroz*, 2002; *Hashimoto and Sugita*, 2003]. Reexamination of previous analyses demonstrated that there may be a significant spatial variation in the surface emissivity as large as $\sim$20% [*Hashimoto and Sugita*, 2003].

[7] Here in this study, we evaluated the Venus surface emissivity at 1.18 μm wavelength using data obtained by the Near-Infrared Mapping Spectrometer (NIMS) aboard the Galileo spacecraft. Because emissivity depends on the mineralogy, a mapping of surface emissivity may constrain the chemical characteristics of the Venus surface. In the following, we first describe the procedure of our analysis which includes the reflection by the planetary surface. Then, we evaluate the surface emissivity, and discuss the errors and assumptions that may affect the estimation. Finally, the existence of paleo-ocean on early Venus is inferred from the spatial variation of surface emissivity.

2. Data and Analysis

2.1. Data

[8] We analyzed the multispectral nightside image identified as VPDIN-1 (for Venus Partial Disk Imaging-NightSide) which covers the disk from approximately 20°W to 90°E longitude [*Carlson and Taylor*, 1993] and is distributed by the Planetary Data System (PDS). Those data were obtained by Galileo NIMS during its flyby of Venus on 10 February 1990. NIMS is an imaging spectrometer, operating in the spectral range from 0.7 to 5.2 μm [*Carlson et al.*, 1992], and images of nightside are obtained with 17 spectral channels [*Carlson et al.*, 1991]. Some channels measured the thermal radiation in the well-known spectral windows at 1.18, 1.74, and 2.3 μm. In these windows, thermal emission originating from both the surface and lower atmosphere are observed [e.g., *Allen and Crawford*, 1984; *Crisp et al.*, 1989; *Carlson et al.*, 1991; *Lecacheux et al.*, 1993; *Pollack et al.*, 1993; *Baines et al.*, 2000].

[9] NIMS channel 3 observed the radiation of the 1.18 μm window, in which thermal emission from the surface leaks through the Venus clouds (Figure 1a). Initial results from the VPDIN observations are described by *Carlson et al.* [1991], which mention that the high-altitude (12 km above mean planetary radius) surface feature Maxwell Montes is detectable in the NIMS channel-3 image. The dark features near the top and the right of the image are likely due to the Ishtar and Aphrodite terra, respectively (Figures 1a and 1e). However, there are also some features irrelevant to the surface. They are probably produced by the effects of scattering by the Venus clouds, which is the dominant effect in channels 5 and 7 (Figures 1c and 1d). Other effects detectable in channel 3 are scattered sunlight and limb darkening. These effects need to be corrected separately.

2.2. Overview of Analysis

[10] The analysis procedure for evaluating surface emissivity is the following. (1) We first remove the contribution of scattered sunlight, (2) we make a correction for emission angle, and (3) we evaluate the surface emissivity. Since the radiation at 1.18 μm window is affected by both clouds and surface topography, these contributions are evaluated to isolate the contribution of surface composition to thermal emissivity.

[11] In this analysis procedure, we use the NIMS channels 4, 5, and 7 in addition to channel 3. Figure 2 provides a schematic representation of the characteristics of radiation observed by the four channels. NIMS channel 4 is used to remove the contribution of scattered sunlight, and the NIMS channels 5 and 7 are used to estimate the cloud properties.

2.3. Radiative Transfer Model

[12] We calculated synthetic spectra by means of a line-by-line radiative transfer program including both scattering and absorption. The computational code was developed by G. L. Hashimoto and others at the University of Tokyo. The algorithm known as the adding method is used to calculate the radiation in a vertically inhomogeneous plane-parallel atmosphere [*Goody and Yung*, 1989]. The number of radiative streams is 12 in each hemisphere. Taking into account a triangular spectral bandpass with the width of 0.025 μm [*Carlson et al.*, 1992], we calculate radiances for each channel from synthesized spectra in which molecular absorption features are resolved.

[13] Following the method by *Pollack et al.* [1993], opacities of gases and particles were calculated. In all our simulations, we used the vertical profiles of gas mixing ratios developed by *Pollack et al.* [1993]. Line absorption data for CO_2, H_2O, CO, SO_2, HF, and OCS were taken from the HITEMP and HITRAN2000 [*Rothman et al.*, 2003; L. S. Rothman et al., HITEMP, the high-temperature molecular spectroscopic database, manuscript in preparation, 2008]. Total internal partition sums (TIPS) are calculated by the TIPS code developed by *Fischer et al.* [2003]. Rayleigh scattering cross sections for atmospheric molecules are calculated from the refractive indices [*Keady and Kilcrease*, 2000; *Penndorf*, 1957; *Vardavas and Carver*, 1984]. Optical properties of cloud particles are calculated by the Mie scattering code [*Bohren and Huffman*, 1983] based on the baseline cloud model [*Pollack et al.*, 1993] and the optical constants of 75% H_2SO_4 solution [*Palmer and Williams*, 1975].

[14] We also introduced a continuum absorption to reproduce an acceptable fit to the NIMS data, since an additional source of continuum opacity is present owing to the far

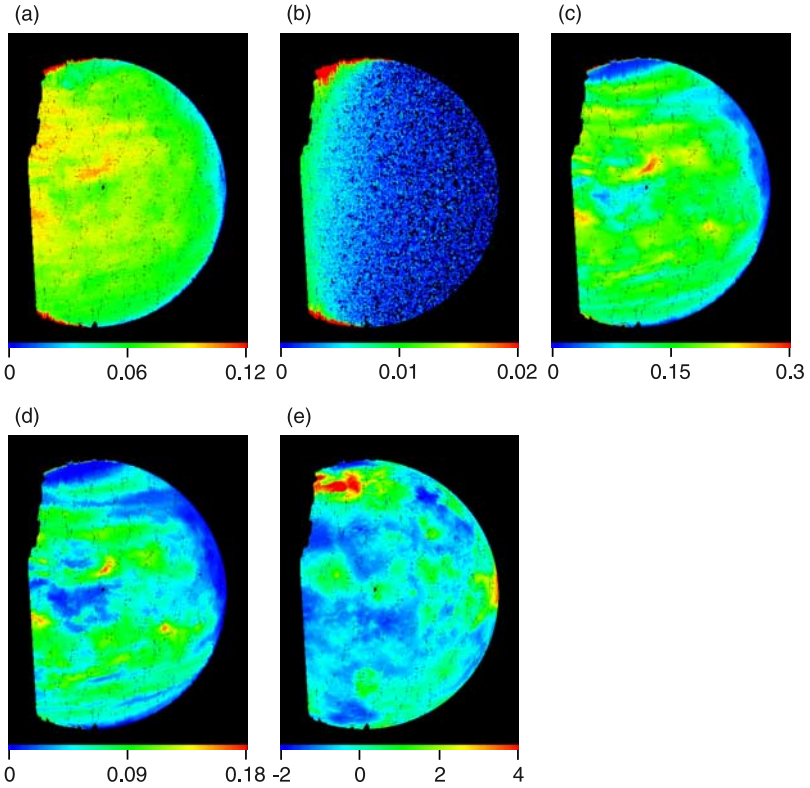

Figure 1. Multispectral images of nightside of Venus. These data were obtained during the first NIMS imaging sequence (VPDIN-1) at a resolution of ~50 km/pixel. (a) An image at 1.18 μm (channel 3). (b) An image at 1.47 μm (channel 4). (c) An image at 1.74 μm (channel 5). (d) An image at 2.31 μm (channel 7). (e) A Magellan topographic map. This image covers from 20°W to 90°E of longitude. The topographic high near the north pole is the Ishtar Terra. The western edge of Ovda Regio can be seen near the rightmost part of the image.

wings of strong CO_2 bands and collision-induced CO_2 opacity [*Pollack et al.*, 1993]. Binary absorption coefficients for continuum opacity are determined to match the measured flux with the cloud model of *Pollack et al.* [1993]. The values used in our simulations are 1.0×10^{-9} cm^{-1} amagat^{-2} for 1.18 μm window, 1.0×10^{-8} cm^{-1} amagat^{-2} for 1.74 μm window, and 7.0×10^{-8} cm^{-1} amagat^{-2} for 2.3 μm window, respectively, though these values are somewhat different

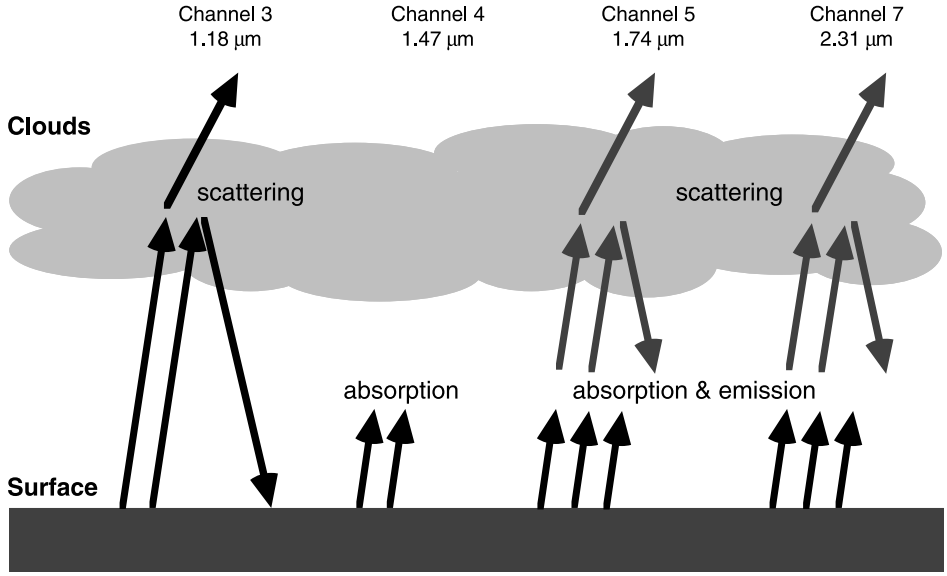

Figure 2. A schematic picture of radiation in Venus's atmosphere and clouds.

from those used in other analyses [e.g., *Bézard et al.*, 1990; *Pollack et al.*, 1993].

2.4. Scattered Sunlight

[15] Nightside emissions at the near-infrared wavelengths contain scattered sunlight reflected off the dayside of the planetary disk. In particular, a strong component that brightens gradually toward the terminator is found in channel 4 (1.47 μm) (Figure 1b). Atmospheric radiative transfer models demonstrate that Venus does not emit thermal radiation at this wavelength. The Venusian CO_2 atmosphere is too opaque to allow radiation to penetrate the atmosphere, though the surface and lower atmosphere of Venus are hot enough to emit thermal radiation at this wavelength. The radiance observed in channel 4 can serve as a good approximation for the scattered sunlight.

[16] We corrected the effect of scattered sunlight, by assuming that the contributions of this effect to channel 3, 5, and 7 are proportional to that of channel 4. Taking into account the solar spectrum, we use the following correction:

$$I_x^S = I_x - \frac{S_x}{S_4} \cdot I_4 \tag{1}$$

where suffix denotes the NIMS channel, I_x^S is the radiance after the correction of scattered sunlight, I_x is the radiance observed by the NIMS, and S_x is the solar spectrum.

2.5. Limb Darkening

[17] We computed limb darkening by using our radiative transfer model. Figure 3 shows our calculated limb darkening curve and NIMS observation that is corrected for the scattered sunlight. The observed limb darkening is well reproduced by our simulation. Although the particle size and number density in the lower clouds would vary in time and space, they affect only scales of radiance and do not affect the shape of limb darkening. Since the upper cloud layer is opaque enough to determine the distribution of emission angle at the cloud top, the shape of limb darkening curve is independent of the property of the lower clouds.

[18] The equation for limb darkening correction is given by

$$I_x^{SL} = \frac{J_x(0)}{J_x(\theta)} \cdot I_x^S \tag{2}$$

where I_x^{SL} is the radiance after the correction of scattered sunlight and limb darkening, $J_x(\theta)$ is the computed radiance for emission angle of θ, respectively.

2.6. Estimation of Surface Emissivity

[19] To evaluate the surface emissivity at 1.18 μm window, we need to take into account the effects of clouds and surface topography. The overlying clouds modulate the radiation mostly by scattering. The lower atmosphere of Venus absorbs the radiation emitted by the surface and also emits thermal radiation, since the opacity of the thick Venus atmosphere is not negligible at 1.18 μm wavelength [e.g., *Taylor et al.*, 1997]. The effects of atmospheric absorption and emission increase with the column density of the atmosphere, which is largely determined by the surface topography owing to hydrostatic balance. For example, the atmospheric column density is smaller in a highland area, leading to smaller atmospheric absorption and emission. In addition the intensity of thermal radiation from the surface is a function of the temperature which in turn decreases with height, so that highlands are cooler and emitting less.

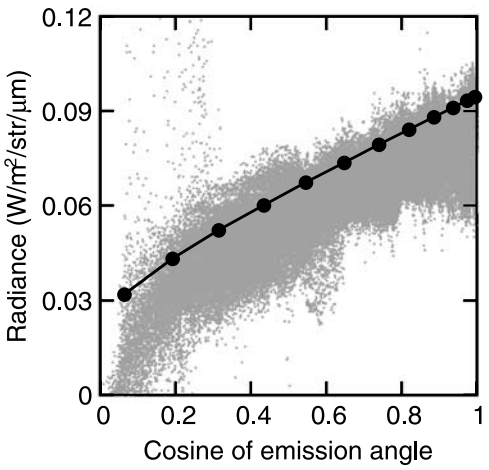

Figure 3. Theoretical and observed limb darkening for the NIMS channel 3. The radiances are plotted as a function of the cosine of the emission angle. The NIMS observation is corrected for the scattered sunlight.

[20] We cannot separate the clouds' correction from the evaluation of surface emissivity, since multiple reflection between the surface and clouds affects the intensity of radiation observed above the clouds [*Hashimoto and Sugita*, 2003]. Here, multiple reflection refers to phenomenon where a fraction of the upward incident radiation at the bottom of cloud layer has experienced reflections between clouds and the planetary surface more than once. This effect has a significant influence on the observed radiance under the Venus conditions, where the reflectivity of overlying clouds is high. Although multiple reflection also occurs on Earth and Mars, the degree of its effect is very small. Since the atmospheric absorption affects the multiple reflection, the correction for modulation induced by clouds is also connected to the surface topography via atmospheric opacity.

[21] To estimate the cloud properties we follow the method of *Carlson et al.* [1993b] which used NIMS channels 5 and 7 (1.74 and 2.31 μm, respectively). At these wavelengths, visible features are almost entirely due to clouds, which modulate the emission from the lower atmosphere, with no significant surface contribution [e.g., *Taylor et al.*, 1997]. It is not necessary to take into account the effect of multiple reflection at these channels, since photons reflected by clouds are absorbed by lower atmosphere (Figure 2). Using the NIMS channel 5 and 7, we can estimate the cloud properties without the influence from the surface emissivity.

[22] Then, we calculate the upward radiance at the top of the atmosphere in channel 3 as a function of surface emissivity. The cloud properties estimated from the NIMS channels 5 and 7 and the surface topography are input to the radiative transfer model. The surface emissivity is evaluated in accordance with the computed relation between

the surface emissivity and the radiance at the top of the atmosphere.

2.6.1. Evaluation of Cloud Properties

[23] The clouds of Venus have been observed by remote sensing as well as in-situ measurement techniques [e.g., *Esposito et al.*, 1983]. The observations indicate that the clouds of Venus are vertically stratified with three layers, which are called the upper, middle, and lower clouds, respectively [e.g., *Knollenberg and Hunten*, 1980]. These clouds are made up of a few different particle size components, which are often referred with mode 1, 2, 2′, and 3 [e.g., *Knollenberg and Hunten*, 1980; *Pollack et al.*, 1993]. The upper and middle clouds are generally uniform and featureless, while considerable spatial variations in cloud properties are observed in the lower cloud [*Marov et al.*, 1980; *Ragent and Blamont*, 1980].

[24] We start with a cloud model developed by *Pollack et al.* [1993] and assume that the spatial variations in cloud properties are caused by variations in the number densities of mode 2′ and 3 particles in the lower clouds. *Carlson et al.* [1993b] demonstrated that the NIMS observation is well reproduced by varying the number densities of mode 2′ and 3 particles. Their results are verified by our radiative transfer model (Figure 4). Since the wavelength dependence of scattering varies with cloud particle size, channels 5 and 7 enable us to distinguish the variation in the abundance of mode 2′ and 3 particles (Figure 5).

2.6.2. Surface Topography and Atmospheric Structure

[25] The surface topography of Venus is measured by the Magellan spacecraft with vertical accuracy of about 50 m [*Pettengill et al.*, 1991]. We assume that the Venusian lower atmosphere is horizontally uniform and the vertical temperature profile is given by the Venus International Reference Atmosphere (VIRA) [*Seiff et al.*, 1985]. Below the zero altitude (6052.0 km from the center of Venus), the temperature lapse rate in the lowermost layer is extrapolated. For pressure extrapolation, the hydrostatic pressure relation is integrated using the temperature profile. We also assume that the temperature of the planetary surface equals to the temperature of atmosphere in contact with it, since the temporal variation of the temperature in the Venusian lower atmosphere is expected to be extremely small [e.g., *Seiff*, 1983].

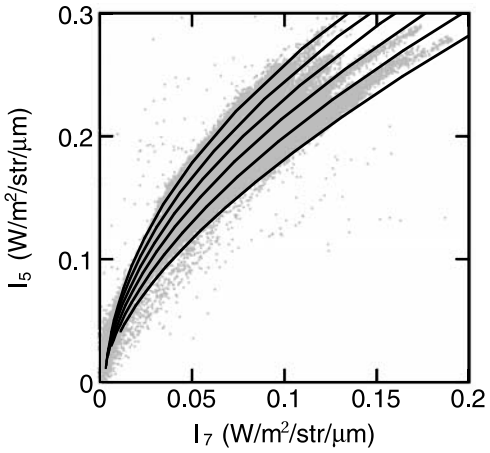

Figure 4. Scatterplot of the NIMS channel 5 against the channel 7. The NIMS data are corrected for the effect of limb darkening. Six theoretical curves are also shown. For each curve, the ratio of mode 3 to mode 2′ content is constant, and the total opacity of the lower cloud is varied. The lowermost curve is for a cloud that contains no mode 3 particles, while the uppermost curve is for a cloud in which the lower cloud is thoroughly composed of mode 3 particles.

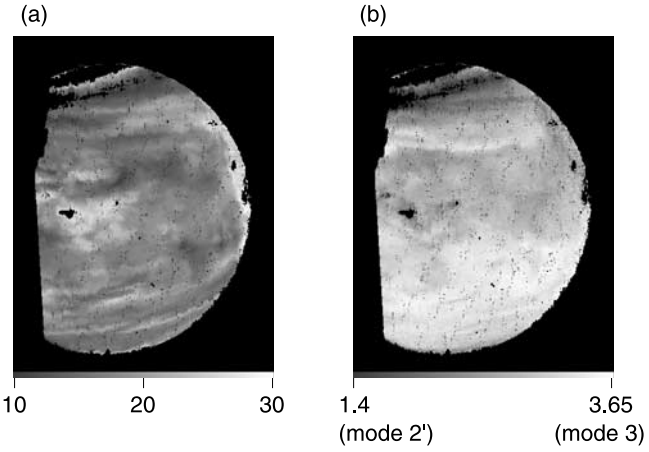

Figure 5. Venus cloud maps. (a) A map of the optical thickness of lower clouds. (b) A map of the modal radius of lower cloud particles.

2.6.3. Emissivity Estimate and Spatial Smoothing

[26] Using our radiative transfer model, we can estimate the surface emissivity based on the band-3 radiance which has been corrected for the effects of scattered day-side light and limb darkening. However, because the band-3 radiance depends only weakly on the surface emissivity due to multiple reflection between clouds and planetary surface [*Hashimoto and Sugita*, 2003], small errors in both observation and correction lead to a large error in surface emissivity estimate. In fact, not all the data points in the band-3 radiance have values that correspond to surface emissivity values between 0 and 1. Thus, we calculated the surface emissivity ϵ beyond the physically significant range (i.e., 0 through 1) by extrapolating the results of radiative transfer model and discarding data points whose ϵ is smaller than -1 or larger than 2. Such a criterion for data selection increases the available data and helps us to obtain a sufficient sample to infer the Venus surface composition. We reduced the random noise by averaging the data within a circle of radius 250 km. This smoothing procedure should not change general trends of the data since the spatial resolution of the Venus surface observation is limited to about 100 km owing to cloud blurring [*Hashimoto and Imamura*, 2001].

3. Results and Discussion

3.1. Surface Emissivity

[27] The estimated surface emissivity at 1.18 μm window wavelength is shown in Figure 6. Although the effect of scattered sunlight increases toward the terminator, our result does not show such a bias. Also there is no noticeable tendency varying with the emission angle, while the effect of limb darkening depends on the emission angle. These facts indicate that both the corrections for the scattered sunlight and limb darkening work fairly well.

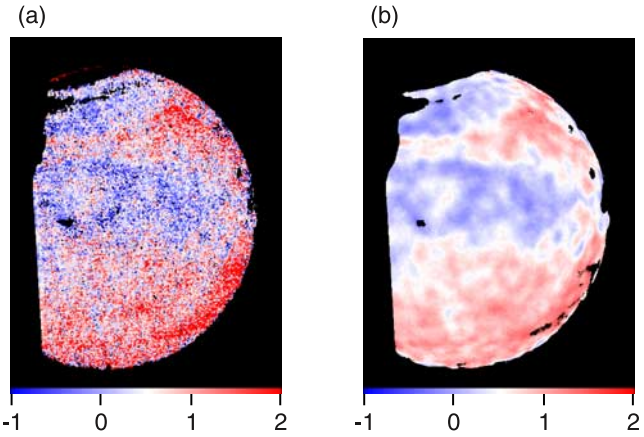

Figure 6. Surface emissivity at 1.18 μm window wavelength. (a) A map of surface emissivity. (b) A map of surface emissivity that is averaged for a region of a circle of radius 250 km.

[28] However, the mean surface emissivity in the Southern Hemisphere is greater than that in the Northern Hemisphere. This feature may be an artifact due to incorrect evaluation of cloud properties, since the modal radius of lower clouds also exhibit such behavior (Figure 5b). The result of declouding that is a correction for this effect is discussed further in section 3.2.

[29] Although the surface emissivity map exhibits a considerable amount of noise, there is a substantial regional variation. For example, Ishtar Terra, Eistla Regio, and Alpha Regio have relatively low emissivity. In contrast, Bell Regio and a band of region from Tahmina Planitia to Fonueha Planitia have higher emissivity values. We will not further discuss a regional difference in emissivity, since surface emissivity estimation might be affected by overlying clouds.

3.2. Declouding

[30] We created a declouded image corrected for cloud-induced contrast (Figure 7a). The cloud-induced contrast was corrected on the basis of the cloud properties evaluated by the method by *Carlson et al.* [1993b]. Although the cloud-induced contrast depends on the surface emissivity, we assumed that surface emissivity is uniform (ϵ = 0.85) during this declouding procedure.

[31] It is clearly shown that all the major features in the topography can be recognized in the declouded image, even though the declouding process is apparently a conspicuous noise source. For comparison, the thermal emission at the NIMS channel 3 wavelength was computed on the basis of the Magellan surface topography, assuming no clouds and uniform surface emissivity (Figure 7b). The correspondence between the declouded image (Figure 7a) and the synthesized image (Figure 7b) indicates that our declouding procedure effectively removes the influence of clouds.

[32] The declouded image shows a north-south asymmetry that is not noticeable before the declouding. Since there is also a hemispheric asymmetry in the modal radius of lower clouds, their appearance of high surface emissivity in the southern hemisphere, especially the region along the limb, might be attributed to insufficient evaluation of cloud properties. However, the Northern Hemisphere does not exhibit such a behavior associated with the modal radius in the lower clouds.

[33] The good fit of Carlson's method (Figure 4) strongly suggests that it works well for evaluating the cloud properties. We did not identify any apparent error in the estimation of surface emissivity, though there may be a problem with the correction for the effect of clouds. It would be an important future work to develop a declouding method that uses the spectra of 1.73 and 2.3 μm window. Some instruments aboard the Venus Express spacecraft are observing the spectra of 1.73 and 2.3 μm window [e.g., *Baines et al.*, 2006], though the Galileo NIMS did not observed them in a mapping mode [*Carlson and Taylor*, 1993].

3.3. Temperature in the Lower Atmosphere

[34] The intensity of leaking radiation at the 1.18 μm window depends not only on the surface emissivity but also on the temperature of lower atmosphere [e.g., *Taylor et al.*, 1997]. A deviation from the assumed temperature profile will cause an error in the surface emissivity estimation. To obtain a rough estimate of the sensitivity to the temperature variation, we computed the intensities of the leaking radiation with varying the temperature of the lower atmosphere. The range of temperature deviation from the VIRA profile is roughly estimated to be about ±2 K, if the spatial variation in the declouded NIMS channel 3 image is entirely attributed to the deviation in the atmospheric temperature.

[35] In other words, our analysis of the NIMS channel 3 indicates that horizontal temperature variation in the lower atmosphere is no more than ±2 K. This is consistent with results from observational and theoretical studies. While measurement accuracies are no less than ±4 K, temperature data from the Venera probes indicated that surface temperatures scatter over no more than a few K [*Seiff et al.*, 1985]. Extrapolation of the temperature profile measured by Pioneer probes indicates surface temperatures from 731 to 735 K [*Seiff et al.*, 1985]. Theoretical study also indicated that variations of temperature in the deep atmosphere is as

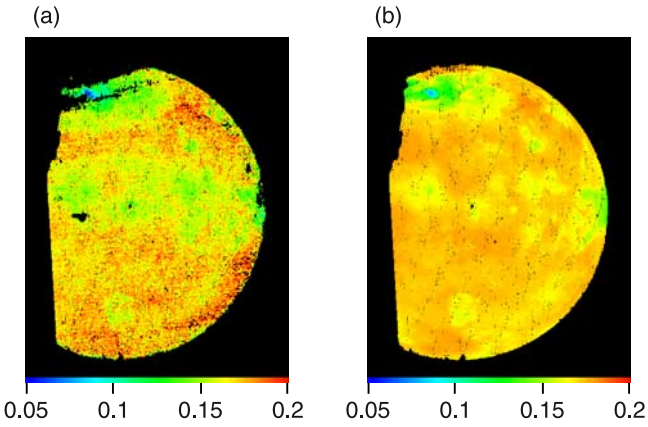

Figure 7. Thermal emission at 1.18 μm window wavelength from the surface and the lower atmosphere. (a) A declouded image that is corrected the cloud-induced contrast. (b) A synthesized image based on the Magellan topographic map.

small as 0.1 K, because of the large heat capacity of the deep atmosphere [*Stone*, 1975].

[36] The NIMS channel 3 image also shows no clear evidence for a variation in temperature in the deep atmosphere with latitude or with local time; temperatures in the deep atmosphere are almost constant in spite of the variation in the insolation as a function of distance from the subsolar point. There might be a small hemispheric asymmetry in the temperature of deep atmosphere causing the north-south asymmetry in the declouded image, though that asymmetry would be attributed to the declouding process. A further study is needed to evaluate the actual horizontal variation in the temperature of deep atmosphere and its influence on the circulation of Venusian atmosphere.

3.4. H_2O Abundance

[37] In the estimation of surface emissivity, we assumed that H_2O mixing ratio is 30 ppmv and is constant below the cloud deck. Since water vapor absorbs some radiation at 1.18 μm window, inhomogeneous distribution of water vapor causes an error in surface emissivity estimation. We computed the intensities of the leaking radiation with varying H_2O mixing ratio, and found that variation of about $\pm$10 ppm in H_2O mixing ratio is required to reproduce the observed contrast in the declouded image.

[38] However, it is unlikely that variation in the H_2O mixing ratio is a major contributer to the spatial variation in the NIMS channel 3 image. Spatial variation of the H_2O abundance in the lower atmosphere had been evaluated by *Drossart et al.* [1993]. They searched for its spatial variations from the analysis of the NIMS complete spectra at maximum spectral resolution using the 1.18 μm window. The result of their analysis is that the water vapor abundance shows no horizontal variation exceeding 20% over a wide latitude range on the nightside of Venus. Hence, the variation in the H_2O mixing ratio is not enough to explain the spatial variation in the NIMS channel 3 image.

3.5. Emissivity and Altitude

[39] Probability densities of surface emissivity (after smoothing) for three different altitude ranges are shown in Figure 8. We can see a general trend of negative correlation between emissivity and altitude; the emissivity of lowlands is generally higher than that of highlands. Although it is difficult to discuss the difference in emissivity in local scales (e.g., a few hundred km) due to noise emerging from the declouding procedure, the majority of lowlands have higher emissivity than the majority of highlands. Whereas there is an uncertainty in the results due to the not well known parameters of the atmosphere, the difference of emisivity between lowlands and highlands is more than 0.3.

[40] The temperature lapse rate of the lowermost atmosphere can cause an altitude-dependent bias in the surface emissivity estimation. When a larger temperature lapse rate was used in the surface emissivity estimation, emissivities of highlands and lowlands are estimated to be higher and lower, respectively. If we use the temperature profile in which the lapse rate of the lowermost atmosphere is about 1 K/km larger than that of VIRA, the difference in the estimated surface emissivity between lowlands and highlands will disappear. However, such a temperature profile

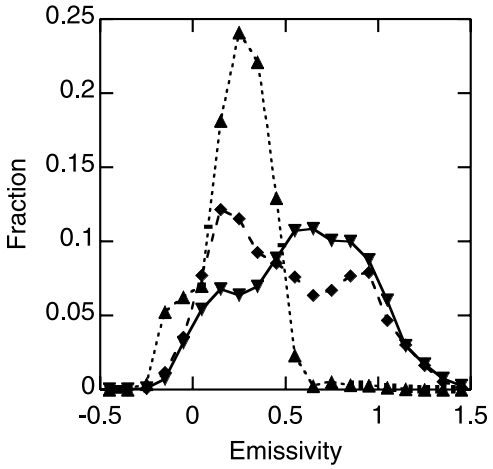

Figure 8. Surface emissivity distribution for three different altitude ranges. Solid curve is for lowlands ($z < 0$ km); dashed curve is for intermediate altitudes (0 km $< z <$ 2 km); and dotted curve is for highlands ($z > 2$ km).

is statically unstable compared with the adiabatic lapse rate [*Seiff et al.*, 1985]. It is unlikely that unstable stratification is observed all over the nightside of Venus, since there is no heat source which maintains the superadiabatic lapse rate.

[41] It is also unlikely that horizontal variations in the H_2O abundance and/or atmospheric temperature cause an altitude-dependent bias in the surface emissivity estimation. If H_2O abundance and/or atmospheric temperature vary in association with surface topography, the estimated emissivity might have a bias related to the altitude. However, no observation indicates that the variation in the H_2O abundance or atmospheric temperature correlates with the surface topography. Thus, it is likely that there is a difference in surface emissivity between lowlands and highlands.

[42] Although we will not argue a regional difference in emissivity, a regional analysis will be useful to test the validity of emissivity estimate independent from any uncertainties in the retrieval. For example, there is no reason to expect that the volcanoes and coronae would be granitic, particularly as they are geologically young (erupted during today's dry Venus). It would be useful to plot the emissivity of the tesserae separately from the other highlands to see if they are similar. Also, a study on the correlation of morphology and retrieved emissivity would be interesting, since morphology of many volcanic structures allows us to infer the chemical composition of the lavas [e.g., *Head et al.*, 1992]. Using the gravity data, we can examine whether there is a systematic difference in emissivity in the same altitude region between isostatically compensated and dynamically supported highlands [e.g., *Smrekar and Phillips*, 1991].

[43] It is worth noting that material properties such as grain size could alter the emissivity, which may correspond to surface roughness or age (older terrains may acquire impact debris over time). It is also possible some differences might be due to weathering or that older terrains are covered by more impact debris which subdues the spectral absorptions. Chemical weathering is a function of altitude, and might be important in connection with anomalous radar

reflectivity [e.g., *Klose et al.*, 1992; *Schaefer and Fegley*, 2004]. These issues will require further consideration.

3.6. CO_2 Continuum Absorption

[44] The opacities of pressure-induced continuum absorption are important and poorly known factor for calculating the emission from the lower levels of the Venus atmosphere. We used the cloud model of *Pollack et al.* [1993] to determine the continuum absorption coefficients, but these values are somewhat different from those used in other analyses [e.g., *Bézard et al.*, 1990; *Pollack et al.*, 1993]. The emissivity contrast between highlands and lowlands revealed by our analysis will decrease with decreasing the continuum opacity. Since more radiation is absorbed above lowlands than above highlands, the decrease in the continuum opacity allows lowlands to emit more radiation. Therefore, smaller continuum opacity leads to an estimation of smaller emissivity in the lowlands. There is still a large uncertainty in the parameters of the clouds, and ambiguity between average cloud opacity and continuum opacity. If the total cloud opacity is larger than that of the Pollack's cloud model, the emissivity difference between highlands and lowlands retrieved by our analysis may decrease or even disappear.

[45] To analyze the thermal emission from the Venus nightside, *Meadows and Crisp* [1996] used a different approach for modeling the CO_2 far wings, instead of a constant binary continuum absorption coefficient. They determined the coefficients of a sub-Lorentzian profile by fitting laboratory data. Assuming constant surface emissivity, they derived that temperature lapse rate is dynamically stable (subadiabatic) as opposed to the dynamically unstable (superadiabatic) lapse rate found in this study. If temperature of the Venusian lower atmosphere is horizontally uniform, the results of *Meadows and Crisp* [1996] indicates a trend of emissivity increasing with altitude. The difference between their and our results indicates that modeling of the CO_2 far wings is crucial to sense the surface and lower atmosphere of Venus.

[46] It is quite obvious that we need detailed modeling and more accurate laboratory measurements for pressure-induced continuum absorption. Although the approach of *Meadows and Crisp* [1996] is no less empirical than the constant binary coefficient, it may provide insights into the processes responsible for the CO_2 continuum absorption. There is also certainly a need for constraining the total cloud opacity. Either by new in situ measurements or possibly by spectroscopy with higher spectral resolution, more reliable estimates of the Venusian surface and lower atmosphere will be obtained.

4. Implication for Venus Geology and Evolution

[47] Near-infrared emissivity can be used to discriminate the rock compositions [e.g., *Ross et al.*, 1969; *Baird*, 1984b]. The emissivity, ϵ, is related to the reflectivity, r, by Kirchhoff's law ($\epsilon = 1 - r$). The reflectance spectra at near-infrared wavelength is most sensitive to the presence of iron-bearing mafic minerals [e.g., *Burns*, 1993]. For mafic rocks with large amounts of mafic minerals, the emissivity around 1 μm is high; while for felsic rocks with small amounts of mafic minerals, the emissivity around 1 μm is low [e.g., *Baird*, 1984a].

[48] Our results indicate that there is a significant difference in emissivity between highlands and lowlands. The relative difference in surface emissivity between lowlands and highlands are consistent with lowlands materials being composed of generally mafic rocks, whereas highlands materials are composed of generally felsic rocks. We cannot yet determine which value of ϵ corresponds to which types of rocks, such as basalt, andesite, and granite. Nevertheless, the observed large disparity in ϵ between the lowland and highland is very difficult to be accounted for by the emissivity variation of basalts alone but requires presence of more felsic rocks, such as granites [e.g., *Hashimoto and Sugita*, 2003].

[49] This inference is consistent with several observations. The radar images of the Venusian surface by Magellan revealed that most landforms in the lowland plains suggest low-viscosity materials, which are characteristic of mafic magmas [e.g., *Head et al.*, 1992]. The data of Venera and Vega landers are interpreted as that lowland materials are dominated by mafic rocks [e.g., *Pieters et al.*, 1986; *Kargel et al.*, 1993]. The inferred composition contrast between lowlands and highlands is also consistent with the principle of isostasy that is the application of Archimedes' principle to the crust. Isostatic compensation at the surface can be achieved either by variation of crustal density or by variation of thickness of homogeneous crust. The estimated emissivity indicates that highland materials are less dense than lowland materials, since density of mafic rocks is higher than that of felsic rocks.

[50] One interpretation for the felsic highland crust is that highlands are composed of granitic rocks. The presence of granitic rocks would imply that Venus had have an ocean and subduction in the past, since it has been suggested that remelting of oceanic crust combined with water along subduction would have caused the formation of granitic magmas [e.g., *Campbell and Taylor*, 1983]. If Venus had been an Earth-like planet where the surface was covered with ocean and subduction processes were working, granitic magmas would be generated like the present Earth. Although the present Venus is a dry-planet where granitic magmas would not be generated any more, ancient continents might have survived until today.

[51] A wet origin for Venus is also suggested by numerical simulations of late-stage accretion which begins after the end of oligarchic growth of planetary embryos [e.g., *Morbidelli et al.*, 2000; *Raymond et al.*, 2004]. Such models indicated that Venus's initial endowment of volatiles is likely similar to that of Earth. In fact, there is similarities between Venus and Earth in the near-surface inventories of carbon and nitrogen [e.g., *Lécuyer et al.*, 2000]. It indicates that Venus's inventory of water was once similar to that of the Earth at the end of planetesimal accretion. In addition, loss of Venus's hydrogen, that is necessary for early wet Venus to evolve into the current dry Venus, is suggested by the hydrogen isotopic ratio (D/H) measured in the atmosphere of Venus [e.g., *DeBergh et al.*, 1991; *Donahue and Hodges*, 1992]. The factor of 100 enrichment in D/H compared to the Earth's ocean is generally considered to be evidence that Venus started with at least 100 times as much hydrogen as it has now [*Donahue et al.*, 1982]. Since early Sun's luminosity is fainter than the present, early Venus

would have avoided going into a state of runaway greenhouse [e.g., *Kasting*, 1988]. If Venus was endowed with sufficient water, early Venus would have had an ocean for more than a billion years [*Hashimoto et al.*, 2007].

[52] It would be an important future work to look for other evidences of ancient ocean on Venus. Unfortunately, we cannot infer the ancient Venus from the observation of Venusian surface morphology, since the age of the Venus surface is no more than 1 billion years [e.g., *Basilevsky et al.*, 1997, and references therein]. However, chemical signatures of water such as hydrous minerals may remain over a longer time period [e.g., *Johnson and Fegley*, 2000], even as the surface morphology has been erased. It is also reasonable to expect that ancient ocean has left its traces in the planetary interior, since the presence of water should have a great influence on the evolution of planets through controlling plate tectonics and mantle convection.

5. Summary

[53] We evaluated the emissivity of the Venus surface at 1.18 μm wavelength using multispectral images obtained by the Galileo NIMS. Although the surface of Venus is shrouded in a thick atmosphere and clouds, our declouding procedure adequately remove the influence of clouds. Our analysis has revealed that the emissivity of lowlands is generally higher than that of highlands. This observation indicates that highland materials are generally composed of felsic rocks, while lowland materials are dominated by mafic rocks. Such a composition contrast between lowlands and highlands is consistent with the principle of isostasy. Since formation of granitic magmas is likely related to water, there is an implication of ancient wet Venus in the presence of granitic terrains.

[54] It would be an important future work to confirm the presence of granitic rocks with the intention of revealing the history of the Venus surface environment. There are five spectral windows in the Venus atmosphere between 0.85 and 1.18 μm that are sensitive to the surface property. We will be able to evaluate the surface emissivity at these spectral windows in the same way as described in this paper. Such spectral information will help us estimate the mineralogic composition of the Venus surface.

[55] It is also worth mentioning that the declouding procedure used in this study is also useful in retrieving temperature profiles in the Venus lower atmosphere. There are several spectral windows in the near-infrared wavelengths that can sense temperatures at several altitude levels below the cloud top. A multilevel global temperature fields retrieved from multiple-wavelength images will provide new insights into the general circulation of the Venus atmosphere.

[56] **Acknowledgments.** The authors express their thanks to anonymous reviewers for their constructive comments on this manuscript. G.L.H. would like to thank Teruyuki Nakajima for detailed discussion of radiative transfer modeling, Naomoto Iwagami for helpful discussion of gas absorption, Yutaka Abe for fruitful discussion of early evolution of terrestrial planets, Yukari Tsutsumi for her help in developing computational code, and Constantine Tsang for his technical aid in preparing figures. G.L.H. and S.S. thank Grants-in-Aid for Scientific Research and The 21st Century COE Program of Origin and Evolution of Planetary Systems of Ministry of Education, Culture, Sports, Science and Technology (MEXT) for support. M.R.S. is supported by Portuguese FCT project PDCTE/FNU/49822/2003 and FCT scholarship BSAB/584/2006.

References

Allen, D. A., and J. W. Crawford (1984), Cloud structure on the dark side of Venus, *Nature*, *307*, 222–224.

Baines, K. H., et al. (2000), Detection of sub-micron radiation from the surface of Venus by Cassini/VIMS, *Icarus*, *148*, 307–311.

Baines, K. H., S. Atreya, R. W. Carlson, D. Crisp, P. Drossart, V. Formisano, S. S. Limaye, W. J. Markiewicz, and G. Piccioni (2006), To the depths of Venus: Exploring the deep atmosphere and surface of our sister world with Venus Express, *Planet. Space Sci.*, *54*, 1263–1278.

Baird, A. K. (1984a), Iron variation within a granitic pluton as determined by near-infrared reflectance, *J. Geol.*, *92*, 344–350.

Baird, A. K. (1984b), Rapid discrimination of granitic rock compositions by low-resolution near-infrared reflectance, *J. Geophys. Res.*, *89*, 2491–2496.

Basilevsky, A. T., J. W. Head, G. G. Schaber, and R. G. Strom (1997), The resurfacing history of Venus, in *Venus II*, edited by S. W. Bougher, D. M. Hunten, and R. J. Phillips, pp. 1047–1084, Univ. of Ariz. Press, Tucson.

Bézard, B., C. de Bergh, D. Crisp, and J.-P. Maillard (1990), The deep atmosphere of Venus revealed by high-resolution night-side spectra, *Nature*, *345*, 508–511.

Bohren, C. R., and D. R. Huffman (1983), *Absorption and Scattering of Light by Small Particles*, 530 pp., John Wiley, New York.

Bullock, M. A., and D. H. Grinspoon (2001), The recent evolution of climate on Venus, *Icarus*, *150*, 19–37.

Burns, R. G. (1993), Origin of electronic spectra of minerals in the visible to near-infrared region, in *Remote Geochemical Analysis: Elemental and Mineralogical Composition*, edited by C. M. Pieters and P. A. J. Englert, pp. 3–29, Cambridge Univ. Press, New York.

Campbell, B. A., R. E. Arvidson, M. K. Shepard, and R. A. Brackett (1997), Remote sensing of surface processes, in *Venus II*, edited by S. W. Bougher, D. M. Hunten, and R. J. Phillips, pp. 503–526, Univ. of Ariz. Press, Tucson.

Campbell, I. H., and S. R. Taylor (1983), No water, no granites — No oceans, no continents, *Geophys. Res. Lett.*, *10*, 1061–1064.

Carlson, R. W., and F. W. Taylor (1993), The Galileo encounter with Venus: Results from the Near-Infrared Mapping Spectrometer, *Planet. Space Sci.*, *41*, 475–476.

Carlson, R. W., et al. (1991), Galileo infrared imaging spectrometer measurements at Venus, *Science*, *253*, 1541–1548.

Carlson, R. W., P. R. Weissman, W. D. Smythe, and J. C. Mahoney (1992), Near-Infrared Mapping Spectrometer experiment on Galileo, *Space Sci. Rev.*, *60*, 457–502.

Carlson, R. W., K. H. Baines, M. Girard, L. W. Kamp, P. Drossart, T. Encrenaz, and F. W. Taylor (1993a), Galileo/NIMS near-infrared thermal imagery of the surface of Venus, *Proc. Lunar Planet. Sci. Conf.*, *24th*, 253.

Carlson, R. W., L. W. Kamp, K. H. Baines, J. B. Pollack, D. H. Grinspoon, T. Encrenaz, P. Drossart, and F. W. Taylor (1993b), Variations in Venus cloud particle properties: A new view of Venus's cloud morphology as observed by the Galileo Near-Infrared Mapping Spectrometer, *Planet. Space Sci.*, *41*, 477–485.

Crisp, D., W. M. Sinton, K. W. Hodapp, B. Ragent, F. Gerbault, J. Goebel, R. Probst, D. Allen, and K. Pierce (1989), The nature of the near-infrared features on the Venus night side, *Science*, *246*, 506–509.

DeBergh, C., B. Bézard, T. Owen, D. Crisp, J.-P. Maillard, and B. L. Lutz (1991), Deuterium on Venus: Observation from Earth, *Science*, *251*, 547–549.

Donahue, T. M., and R. R. Hodges Jr. (1992), Past and present water budget of Venus, *J. Geophys. Res.*, *97*, 6083–6091.

Donahue, T. M., J. H. Hoffman, R. R. Hodges Jr., and A. J. Watson (1982), Venus was wet: A measurement of the ratio of D to H, *Science*, *216*, 630–633.

Drossart, P., et al. (1993), Search for spatial variations of the H_2O abundance in the lower atmosphere of Venus from NIMS-Galileo, *Planet. Space Sci.*, *41*, 495–504.

Esposito, L. W., R. G. Knollenberg, M. Y. Marov, O. B. Toon, and R. P. Turco (1983), The clouds and hazes of Venus, in *Venus*, edited by D. M. Hunten et al., pp. 484–564, Univ. of Ariz. Press, Tucson.

Fischer, J., R. R. Gamache, A. Goldman, L. S. Rothman, and A. Perrin (2003), Total internal partition sums for molecular species in the 2000 edition of the HITRAN database, *J. Quant. Spectrosc. Radiat. Transfer*, *82*, 401–412.

Goody, R. M., and Y. L. Yung (1989), *Atmospheric Radiation*, 519 pp., Oxford Univ. Press, Oxford, U. K.

Hashimoto, G. L., and Y. Abe (2000), Stabilization of Venus' climate by a chemical-albedo feedback, *Earth Planets Space*, *52*, 197–202.

Hashimoto, G. L., and Y. Abe (2005), Climate control on Venus: Comparison of the carbonate and pyrite models, *Planet. Space Sci.*, *53*, 839–848.

Hashimoto, G. L., and T. Imamura (2001), Elucidating the rate of volcanism on Venus: Detection of lava eruptions using near-infrared observations, *Icarus*, *154*, 239–243.

Hashimoto, G. L., and S. Sugita (2003), On observing the compositional variability of the surface of Venus using nightside near-infrared thermal radiation, *J. Geophys. Res.*, *108*(E9), 5109, doi:10.1029/2003JE002082.

Hashimoto, G. L., Y. Abe, and S. Sugita (2007), The chemical composition of the early terrestrial atmosphere: Formation of a reducing atmosphere from CI-like material, *J. Geophys. Res.*, *112*, E05010, doi:10.1029/2006JE002844.

Head, J. W., L. S. Crumpler, J. C. Aubele, J. E. Guest, and R. S. Saunders (1992), Venus volcanism: Classification of volcanic features and structures, associations, and global distribution from Magellan data, *J. Geophys. Res.*, *97*, 13,153–13,198.

Johnson, N. M., and B. Fegley Jr. (2000), Water on Venus: New insights from tremolite decomposition, *Icarus*, *146*, 301–306.

Kargel, J. S., G. Komatsu, V. R. Baker, and R. G. Strom (1993), The volcanology of Venera and VEGA landing sites and the geochemistry of Venus, *Icarus*, *103*, 253–275.

Kasting, J. F. (1988), Runaway and moist greenhouse atmospheres and the evolution of Earth and Venus, *Icarus*, *74*, 472–494.

Keady, J. J., and D. P. Kilcrease (2000), Radiation, in *Allen's Astrophysical Quantities*, edited by A. N. Cox, pp. 95–120, Springer, New York.

Klose, K. B., J. A. Wood, and A. Hashimoto (1992), Mineral equilibria and the high radar reflectivity of Venus mountaintops, *J. Geophys. Res.*, *97*, 16,353–16,369.

Knollenberg, R. G., and D. M. Hunten (1980), The microphysics of the clouds of Venus: Results of the Pioneer Venus particle size spectrometer experiment, *J. Geophys. Res.*, *85*, 8039–8058.

Lecacheux, J., P. Drossart, P. Laques, F. Deladerrière, and F. Colas (1993), Detection of the surface of Venus at 1.0 μm from ground-based observations, *Planet. Space Sci.*, *41*, 543–549.

Lécuyer, C., L. Simon, and F. Guyot (2000), Comparison of carbon, nitrogen and water budgets on Venus and the Earth, *Earth Planet. Sci. Lett.*, *181*, 33–40.

Marov, M. Y., V. E. Lystsev, V. N. Lebedev, N. L. Lukashevich, and V. P. Shari (1980), The structure and microphysical properties of the Venus clouds: Venera 9, 10 and 11 data, *Icarus*, *44*, 608–639.

Meadows, V. S., and D. Crisp (1996), Ground-based near-infrared observations of the Venus nightside: The thermal structure and water abundance near the surface, *J. Geophys. Res.*, *101*, 4595–4622.

Morbidelli, A., J. Chambers, J. I. Lunine, J. M. Petit, F. Robert, G. B. Valsecchi, and K. E. Cyr (2000), Source regions and timescales for the delivery of water to the Earth, *Meteorit. Planet. Sci.*, *35*, 1309–1320.

Moroz, V. I. (2002), Estimates of visibility of the surface of Venus from descent probes and balloons, *Planet. Space Sci.*, *50*, 287–297.

Palmer, K. F., and D. Williams (1975), Optical constants of sulfuric acid: Application to the clouds of Venus?, *Appl. Opt.*, *14*, 208–219.

Penndorf, R. (1957), Tables of the refractive index for standard air and the Rayleigh scattering coefficient for the spectral region between 0.2 and 20.0 μ and their application to atmospheric optics, *J. Opt. Soc. Am.*, *47*, 176–182.

Pettengill, G. H., P. G. Ford, and S. Nozette (1982), Venus: Global surface radar reflectivity, *Science*, *217*, 640–642.

Pettengill, G. H., P. G. Ford, W. T. K. Johnson, R. K. Raney, and L. A. Soderblom (1991), Magellan: Radar performance and data products, *Science*, *252*, 260–265.

Pettengill, G. H., P. G. Ford, and R. J. Wilt (1992), Venus surface radiothermal emission as observed by Magellan, *J. Geophys. Res.*, *97*, 13,091–13,102.

Pettengill, G. H., B. A. Campbell, D. B. Campbell, and R. A. Simpson (1997), Surface scattering and dielectric properties, in *Venus II*, edited by S. W. Bougher, D. M. Hunten, and R. J. Phillips, pp. 527–546, Univ. of Ariz. Press, Tucson.

Pieters, C. M., et al. (1986), The color of the surface of Venus, *Science*, *234*, 1379–1383.

Pollack, J. B., et al. (1993), Near-infrared light from Venus' nightside: A spectroscopic analysis, *Icarus*, *103*, 1–42.

Ragent, B., and J. Blamont (1980), The structure of the clouds of Venus: Results of the Pioneer Venus nephelometer experiment, *J. Geophys. Res.*, *85*, 8015–8089.

Raymond, S. N., T. Quinn, and J. I. Lunine (2004), Making other earths: Dynamical simulations of terrestrial planet formation and water delivery, *Icarus*, *168*, 1–17.

Ross, H. P., J. E. M. Adler, and G. R. Hunt (1969), A statistical analysis of the reflectance of igneous rocks from 0.2 to 2.65 microns, *Icarus*, *11*, 46–54.

Rothman, L. S., et al. (2003), The HITRAN molecular spectroscopic database: Edition of 200 0 including updates through 2001, *J. Quant. Spectrosc. Radiat. Transfer*, *60*, 665–710.

Schaefer, L., and B. Fegley Jr. (2004), Heavy metal frost on Venus, *Icarus*, *168*, 215–219.

Seiff, A. (1983), Thermal structure of the atmosphere of Venus, in *Venus*, edited by D. M. Hunten et al., pp. 215–279, Univ. of Ariz. Press, Tucson.

Seiff, A., J. T. Schofield, A. J. Kliore, F. W. Taylor, S. S. Limaye, H. E. Revercomb, L. A. Sromovsky, V. V. Kerzhanovich, V. I. Moroz, and M. Y. Marov (1985), Models of the structure of the atmosphere of Venus from the surface to 100 kilometers altitude, *Adv. Space Res.*, *5*, 3–58.

Smrekar, S. E., and R. J. Phillips (1991), Venusian highlands — Geoid to topography ratios and their implications, *Earth Planet. Sci. Lett.*, *107*, 582–597.

Stone, P. H. (1975), The dynamics of the atmosphere of Venus, *J. Atmos. Sci.*, *32*, 1005–1016.

Surkov, Y. A., V. L. Barsukov, L. P. Moskalyeva, V. P. Kharyukova, and A. L. Kemurdzhian (1984), New data on the composition, structure, and properties of Venus rock obtained by Venera 13 and Venera 14, *Proc. Lunar Planet. Sci. Conf. 14th, Part 2, J. Geophys. Res.*, *89*, suppl., B393–B402.

Surkov, Y. A., L. P. Moskalyova, V. P. Kharyukova, A. D. Dudin, G. G. Smirnov, and S. Y. Zaitseva (1986), Venus rock composition at the Vega 2 landing site, *Proc. Lunar Planet. Sci. Conf. 17th, Part 1, J. Geophys. Res.*, *91*, suppl., E215–E218.

Surkov, Y. A., F. F. Kirnozov, V. N. Glazov, A. G. Dunchenko, L. P. Tatsy, and O. P. Sobornov (1987), Uranium, thorium, and potassium in the Venusian rocks at the landing sites of Vega 1 and 2, *Proc. Lunar Planet. Sci. Conf. 17th, Part 2, J. Geophys. Res.*, *92*, suppl., E537–E540.

Taylor, F. W., D. Crisp, and B. Bézard (1997), Near-infrared sounding of the lower atmosphere of Venus, in *Venus II*, edited by S. W. Bougher, D. M. Hunten, and R. J. Phillips, pp. 325–351, Univ. of Ariz. Press, Tucson.

Vardavas, I. M., and J. H. Carver (1984), Solar and terrestrial parameterizations for radiative-convective models, *Planet. Space Sci.*, *32*, 1307–1325.

K. H. Baines, R. W. Carlson, and L. W. Kamp, Jet Propulsion Laboratory, California Institute of Technology, M/S 183-601, 4800 Oak Grove Drive, Pasadena, CA 91109, USA. (kbaines@scn.jpl.nasa.gov; rcarlson@lively.jpl.nasa.gov; lwk@mipl.jpl.nasa.gov)

M. S. Gilmore, Department of Earth and Environmental Sciences, Wesleyan University, 265 Church Street, Middletown, CT 06459, USA. (mgilmore@wesleyan.edu)

G. L. Hashimoto, Laboratory for Earth and Planetary Atmospheric Science, Organization of Advanced Science and Technology, Kobe University, 1-1 Rokkodai, Nada, Kobe 657-8501, Japan. (george@kobe-u.ac.jp)

M. Roos-Serote, Lisbon Astronomical Observatory, Tapada da Ajuda, P-1349-018, Lisbon, Portugal. (maarten@lightcurvefilms.com)

S. Sugita, Department of Complexity Science and Engineering, Graduate School of Frontier Science, University of Tokyo, 5-1-5 Kashiwanoha, Kashiwa, Chiba, 277-8561, Japan. (sugita@k.u-tokyo.ac.jp)